analytical chemistry

pubs.acs.org/ac Article

Oxidase-like ZnCoFe Three-Atom Nanozyme as a Colorimetric Platform for Ascorbic Acid Sensing

Rufen Wu,[#] Mengru Sun,[#] Xiaolong Liu,[#] Fengjuan Qin, Xinyu Zhang, Zhenni Qian, Juan Huang, Yujing Li, Ting Tan,* Wenxing Chen,* and Zhengbo Chen*

Cite This: *Anal. Chem.* 2022, 94, 14308−14316 Read Online

ACCESS | Metrics & More | Article Recommendations | Supporting Information

ABSTRACT: Great enthusiasm in single-atom catalysts for various catalytic reactions continues to heat up. However, the poor activity of the existing single/dual-metal-atom catalysts does not meet the actual requirement. In this scenario, the precise design of triple-metal-atom catalysts is vital but still challenging. Here, a triple-atom site catalyst of FeCoZn catalyst coordinated with S and N, which is doped in the carbon matrix (named FeCoZn-TAC/SNC), is designed. The FeCoZn catalyst can mimic the activity of oxidase by activating O_2 into $^{\bullet}O_2^-$ radicals by virtue of its atomically dispersed metal active sites. Employing this characteristic, triple-atom catalysts can become a great driving force for the development of novel biosensors featuring adequate sensitivity. First, the property of FeCoZn catalyst as an oxidase-like nanozyme was explored. The obtained FeCoZn-TAC/SNC shows remarkably enhanced catalytic performance than that of FeCoZn-TAC/NC and single/dual-atom site catalysts (FeZn, CoZn, FeCo-DAC/NC and Fe, Zn, Co-SAC/NC) because of trimetallic sites, demonstrating the synergistic effect. Further, the utility of the oxidase-like FeCoZn-TAC/SNC in biosensor field is evaluated by the colorimetric sensing of ascorbic acid. The nanozyme sensor shows a wide concentration range from 0.01 to 90 μM and an excellent detection limit of 6.24 nM. The applicability of the nanozyme sensor in biologically relevant detection was further proved in serum. The implementation of TAC in colorimetric detection holds vast promise for further development of biomedical research and clinical diagnosis.

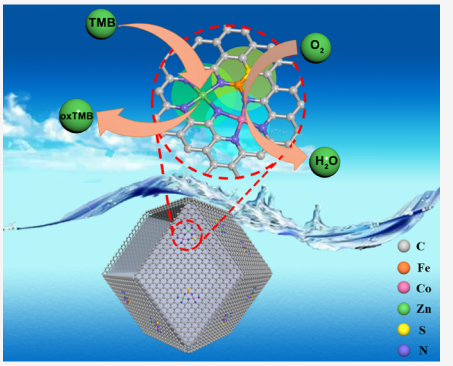

INTRODUCTION

Ascorbic acid (AA), commonly known as vitamin C, as one of the important vitamins to adjust the normal physiological function of the body, participates in different types of reactions of the body. AA also has antioxidant capacity, resists free radical damage to cells, and effectively avoids obstacles to cell regeneration.[1−3] AA has been reported to be implicated with many diseases, such as scurvy, anemia, arteriosclerosis, ischemic stroke, cardiovascular disease, and so forth.[4] Thus, it is vital to develop sensitive and fast methods for dynamically monitoring the AA level in living systems. In body fluids, AA is mainly contained in blood and urine. The AA content per 100 g of white blood cells was 1.425−1.710 mmol as measured by the platelet layer of white blood cells. The content of AA in 24 h urine was 20−40 mg. Thus far, various elegant technologies and methods, including high-performance liquid chromatography combined with electrochemical detector, micromachined electrophoresis chip, gas chromatography-mass spectrometry, capillary electrophoresis, colorimetry, electrochemistry, and fluorescence, have been used for the detection of AA.[5−9] Among them, the colorimetric assay technique was popular because of the advantages of simplicity, rapidity, low cost, and visibility.[10−12]

Nanozymes are usually defined as nanomaterials with intrinsic enzyme-like characteristics. Because they can solve the shortcomings of traditional enzymes, including variability, high preparation cost, and limited practical applications, they have attracted great interest.[13−15] In recent years, many nanozymes have become promising for biosensing because they possess an intrinsic horseradish peroxidase-mimicking activity toward the oxidation of common chromogenic substances such as ophenylenediamine, 3,3′,5,5′-tertamethylbenzidine (TMB), and di-azo-aminobenzene.[16,17] Although great stride has been made in nanozymes, the activity of these nanozymes is far lower than that of natural enzymes. Since being reported by Zhang group in 2011,[18] single-atom catalysts (SACs) have sprung up in the field of catalysis. These SACs with the "soul" of homogeneous catalysts and the "body" of heterogeneous catalysts succeed in the advantages of both homogeneous and heterogeneous catalysts[19,20] and have been considered to be a promising candidate for simulating the catalytic sites of metalloenzymes.[21−25] However, designing a unified structure

Received: July 2, 2022
Accepted: September 20, 2022
Published: October 4, 2022

https://doi.org/10.1021/acs.analchem.2c02853
Anal. Chem. 2022, 94, 14308−14316

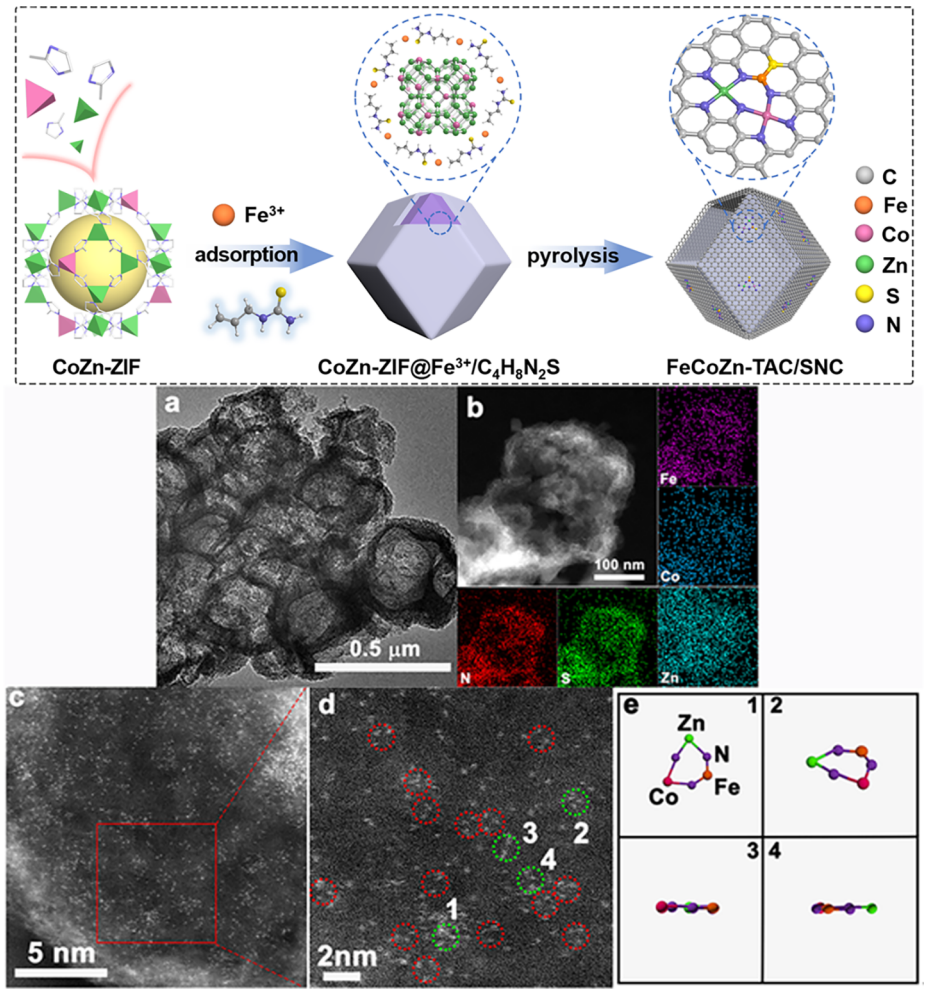

Figure 1. Schematic illustration for the preparation of FeCoZn-TAC/SNC. (a) TEM image, (b) EDS images, (c) HAADF-STEM image, and (d) enlarged HAADF-STEM image of FeCoZn-TAC/SNC. (e) Distribution of three atoms at different angles corresponding to (d).

containing different atomic active sites (>2) to achieve the synergistic effect among them on catalytic reactions is still a pivotal challenge.

Intrigued by the advantages of SACs and scanty research on triple-atom catalysts (TACs), herein, for the first time, we design and synthesize novel FeCoZn TACs with Fe, Co, and Zn three-atom sites anchored on porous concave S- and N-doped carbon matrix. With the capability to catalyze the conversion of O_2 into $^{\bullet}O_2^-$ radicals, FeCoZn TACs can initiate some discoloration reactions. Based on this, the FeCoZn TACs can act as an efficient catalyst with remarkable oxidase-like activity for AA sensing in serum with high sensitivity and selectivity, thus endowing great potential to TACs for biomedical applications. Density functional theory (DFT) calculations further indicate that the isolated Fe, Co, and Zn atoms not only act as the active center of TMB oxidation but also synergically boost spatial charge separation and transfer of the hybrid. The Fe−S_1N_2 and Co_1−N_4 moieties were beneficial to bonding with O_2, while the Zn_1−N_4 centers serve as efficient adsorption sites for nitrogen atoms in TMB molecules. To our knowledge, FeCoZn TACs represent a distinctive case of a triple-atom active site discrete coordination architecture for effective oxidase-like catalytic activity.

EXPERIMENTAL SECTION

Materials. 3,3′,5,5′-tetramethylbenzidine (TMB), ascorbic acid (AA), aspartic acid (Asp), arginine (Arg), methionine (Met), glutamic acid (Glu), histidine (his), and lysine (Lys) were obtained from Sigma-Aldrich (Shanghai, China). Zinc nitrate hexahydrate (99.5%), $FeCl_3$ (98%), dicyandiamide (DCDA), and trimesic acid were purchased from Alfa Aesar. Cobalt nitrate hexahydrate (99%) was purchased from Aladdin. 2-Methylimidazole (98%) and allylthiourea (98%) were purchased from Innochem. Methanol (99.5%) and ethanol (99.5%) were purchased from Sinopharm Group. Sulfuric acid (H_2SO_4) (98%) was purchased from Beijing Chemical Reagent. All experiments used ultrapure water (Millipore Milli-Q grade) with a resistivity of 18.2 MΩ cm. All the reagents were of analytical grade.

Instrumentation. The morphology of the catalyst was monitored by transmission electron microscopy (TEM, JEOL JEM-2100F microscope). The high-angle annular dark-field scanning transmission electron microscopy (HAADF-STEM) images and energy dispersive X-ray spectroscopy (EDS) elemental mapping were measured by a JEOL ARM-200 microscope operating at a voltage of 200 kV, equipped with a probe spherical corrector. The Fe, Co, and Zn K-edge X-ray absorption fine spectroscopy (XAFS) data were obtained at station BL14W1 of Shanghai Synchrotron Radiation Facility

https://doi.org/10.1021/acs.analchem.2c02853
Anal. Chem. 2022, 94, 14308−14316

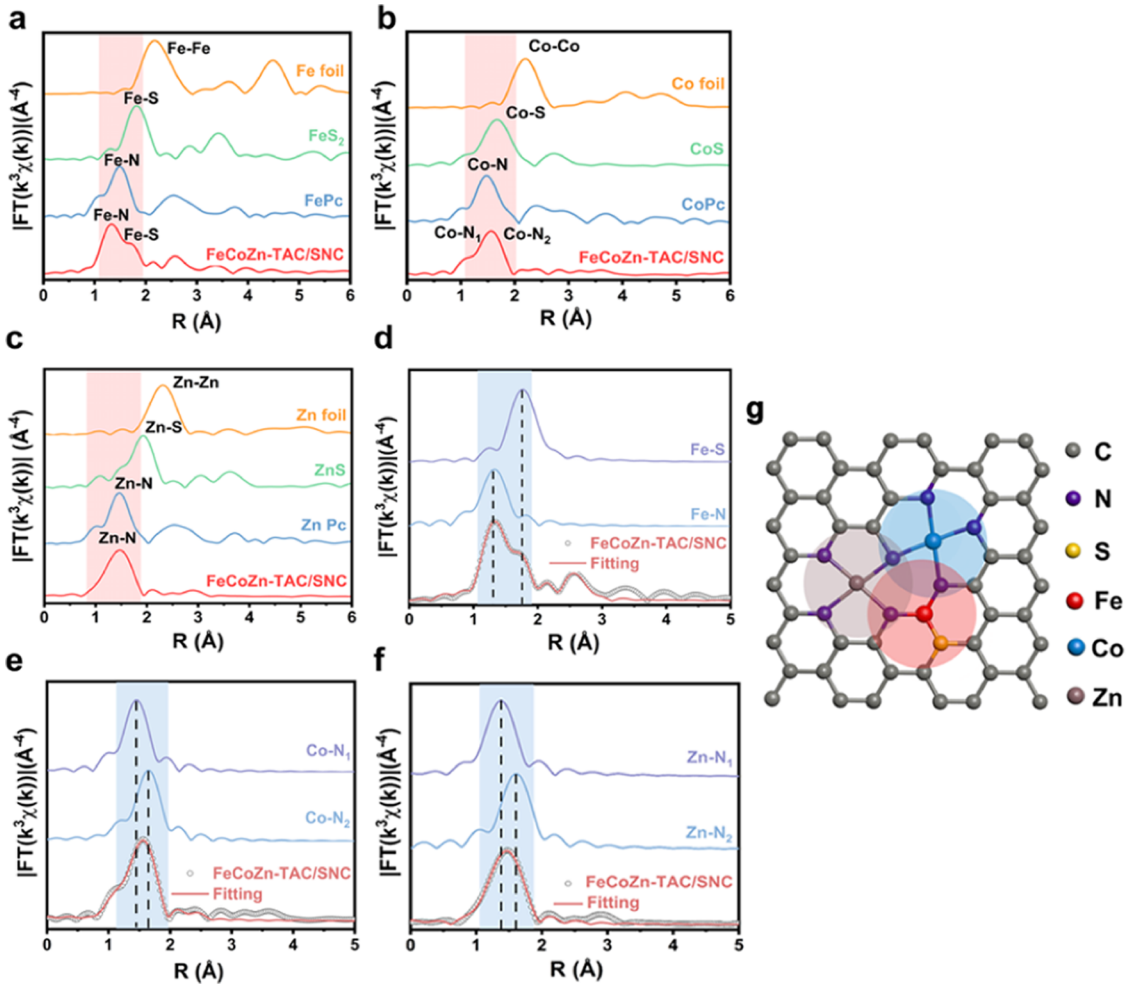

Figure 2. (a) Fe, (b) Co, and (c) Zn K-edge EXAFS spectra of FeCoZn-TAC/SNC and references. (d,e) FT-EXAFS fittings at R space of (d) Fe K-edge, (e) Co K-edge, and (f) Zn K-edge. (f) Obtained structure of FeCoZn-TAC/SNC.

(SSRF, operated at 3.5 GeV, maximum current of 250 MA). UV−vis absorption spectra were acquired by a UV-2550 spectrophotometer (Shimadzu, Japan).

Synthesis of the FeCoZn-TAC/SNC. 0.382 g of dried CoZn-ZIF was dispersed in 20 mL of methanol, and then 5 mg of $FeCl_3$ and 1 g of allylthiourea were added to the mixture, stirred vigorously for 5 min, and heated at 80 °C for 2 h. Then, the precipitate was collected by centrifugation and dried in a vacuum oven at 80 °C to obtain a powder. Finally, the powder was calcined in a tube furnace under an inert atmosphere for 180 min to form FeCoZn-TAC/SNC. The heating rate of the carbonization process was 4 °C/min.

Procedure for Colorimetric Detection of AA. To a 1.5 mL microtube, 100 μL of 12 μg/mL FeCoZn-TAC/SNC, 100 μL of 0.4 mM TMB, and 100 μL of AA with different concentrations were sequentially added. Subsequently, the pH of the mixture solution was adjusted to 4.2 by using 100 μL of 1 M HAc-NaAc solution. Next, the resulting solution was further diluted with deionized water, and a final reaction volume was maintained at 1 mL, followed by incubation at room temperature for 10 min. The UV−vis absorption spectra of the resultant solutions were recorded using a UV−vis photometer, and the corresponding optical images were collected by a digital camera.

Procedure for Colorimetric Detection of AA in Human Serum. The serum samples were collected from PLA General Hospital. The serum samples were filtered and diluted 100 times with HAc-NaAc buffer (pH 4.2, 1 M). Then, the diluted water samples were spiked with 0.1, 1, 10, 50, 60, 70, 80, 90, and 100 μM AA, and the detailed procedure of the colorimetric assay referred to that for the model AA just by adding the diluted human serum instead of the AA standard solution.

Calculation Details. The Vienna Ab-initio Simulation Package[26−29] was used to perform the spin-polarized DFT calculations. The Projected Augmented Waves method and Perdew−Burke−Ernzerhof (PBE)[30] exchange-correlation functional were adopted. Grimme's DFT-D3[31,32] method was employed, accounting for the long-range interaction. The geometries for the reaction intermediates were fully optimized with a 400 eV energy cutoff with lattice parameters fixed and a Gamma-centered *k*-point mesh of 1 × 3 × 1. The energetics were further refined with the implicit water solvation model.

Of note, we acknowledge that the planewave-based periodic DFT fails to correctly describe cations. The protonation is predicted to promote the desorption of oxTMB with periodic DFT-PBE. These steps involving cations were further examined in Gaussian 09 package. We adopted the DFT-M06-L/GENECP method to investigate the reaction energies with cations. The cation-related reactions are reactions A4, A7, A10, A14, and B3, as noted in Table S2, all of which are the protonation/desorption of oxTMB. Here, take reaction A4 as an example. In order to analyze the effect of protonation, a cluster

https://doi.org/10.1021/acs.analchem.2c02853
Anal. Chem. 2022, 94, 14308−14316

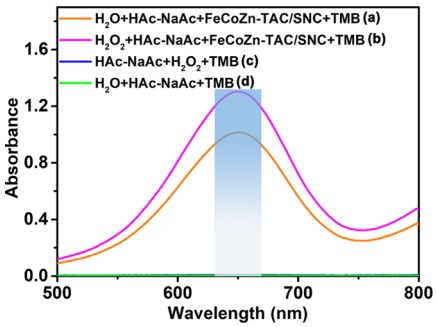

Figure 3. UV−vis absorption spectra of the solutions containing (a) H_2O-HAc-NaAc-FeCoZn-TAC/SNC-TMB, (b) H_2O_2-HAc-NaAc-FeCoZn-TAC/SNC-TMB, (c) HAc-NaAc-H_2O_2-TMB, and (d) H_2O-HAc-NaAc-TMB.

($C_{83}H_{24}N_7SCoFeZn$) as shown in Figure S14 was cut along the FeCoZn/SN edge and additionally surrounded by carbon atoms. The dangling bonds were saturated with hydrogen atoms. The geometries and energies of this cluster were optimized at the DFT-M06-L/GENECP level (6-31G* for C, N, O, S and H; LANL2DZ for Fe, Co, and Zn). The oxTMB may release from the catalyst without the protonation as reaction S1. The desorption energy ΔE_1 is predicted to be 1.49 and 0.97 eV with periodic DFT-PBE and DFT-M06-L, respectively. However, the desorption energy of protonated oxTMB is −0.24 eV by periodic DFT-PBE and −1.38 eV by DFT-M06-L. The DFT-M06-L method further confirms that the protonation of oxTMB forming $oxTMB^+$ significantly promotes the desorption.

*FeO*CoOH*ZnoxTMB + H_3O^+ = *FeO*CoOH + H_2O + $oxTMB^+$ (A4, ΔE)

*FeO*CoOH*ZnoxTMB = *FeO*CoOH + oxTMB (S1, ΔE_1)

These results indicate that the desorption of protonated oxTMB exhibits relatively low energy cost and is not the determining step of the catalytic process.

RESULTS AND DISCUSSION

Characterization of FeCoZn-TAC/SNC. The synthesis process of FeCoZn-TAC/SNC is shown in Figure 1. Then, the morphology and element distribution of FeCoZn-TAC/SNC were characterized. The TEM (Figure 1a) image shows that FeCoZn-TAC/SNC has a hollow porous structure. Meanwhile, no metal nanoparticles were observed on the carbon matrix. The EDS images display the homogeneous distribution of Fe, Co, Zn, S, and N throughout the carbon matrix (Figure 1b). The

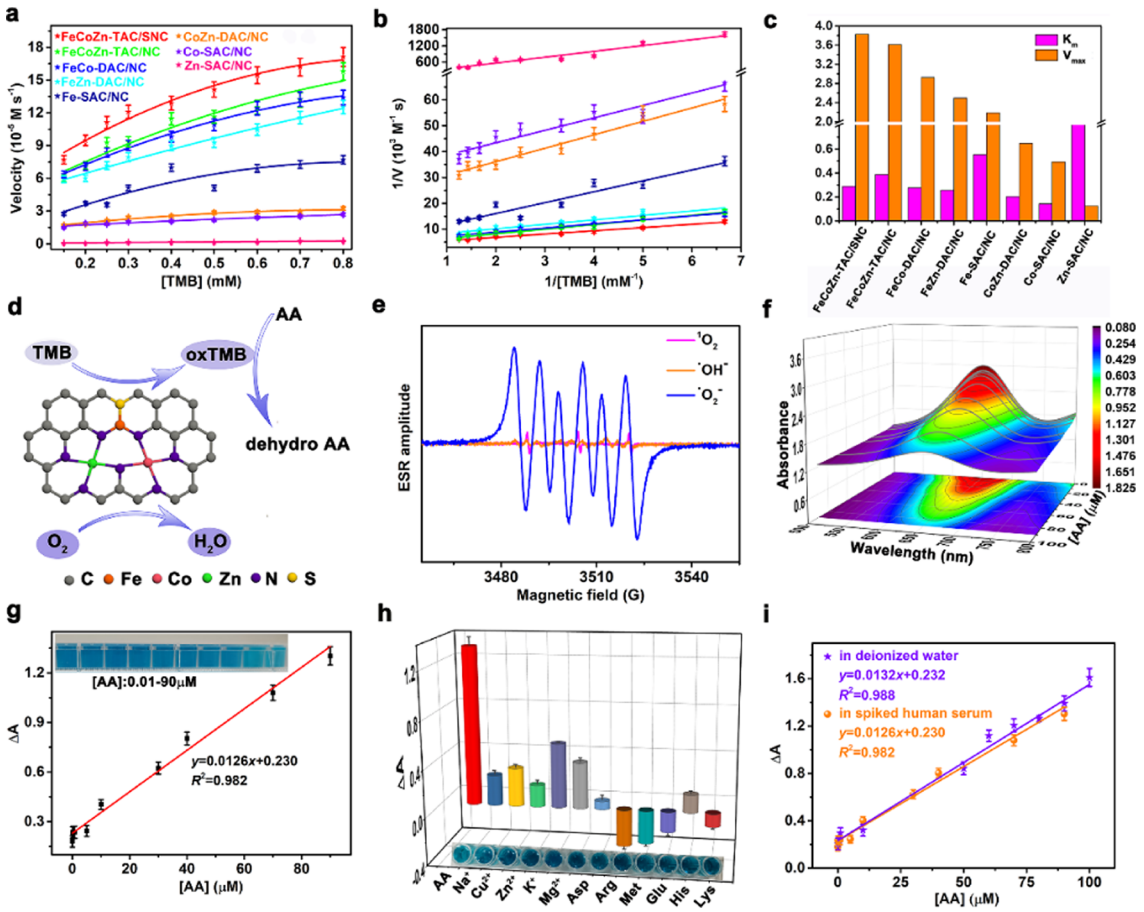

Figure 4. Oxidase-like performance of FeCoZn-TAC/SNC. (a) Michaelis−Menten curves with different concentrations of TMB. (b) Double reciprocal Lineweaver−Burk plot of activity. (c) Comparison of oxidase-like activity of FeCoZn-TAC/SNC with references. (d) Schematic illustration of the colorimetric assay for AA sensing based on the FeCoZn-TAC/SNC -TMB-O_2 reaction system. (e) ESR spectra of FeCoZn-TAC/SNC for ROS generations by using 5,5-dimethyl-1-pyrroline N-oxide (DMPO) as a spin trapping agent. (f) UV−vis absorption spectra of the FeCoZn-TAC/SNC-TMB-O_2 reaction system with different concentrations of AA. (g) Linear calibration curve for colorimetric detection of AA. (h) Absorbance changes caused by different interferents, each at a concentration of 1 mM and AA at 0.1 mM. (i) Absorbance response of the assay to AA spiked in deionized water and serum. Each point represents the average of triplicate determinations.

https://doi.org/10.1021/acs.analchem.2c02853
Anal. Chem. 2022, 94, 14308−14316

Table 1. Comparison of Oxidase-like Activity of FeCoZn-TAC/SNC with References

catalysts	substrate	K_m (mM)	V_{max} (10^{-7} M s^{-1})	ref
FeCoZn-TAC[a]/SNC	TMB	0.459	2.230	this work
FeCoZn-TAC/NC	TMB	0.278	1.262	this work
CoZn-DAC[b]/NC	TMB	0.445	1.425	this work
FeZn-DAC/NC	TMB	0.293	1.040	this work
FeCo-DAC/NC	TMB	0.399	0.936	this work
Fe-SAC[c]/NC	TMB	0.347	0.889	this work
Co-SAC/NC	TMB	0.348	0.242	this work
Zn-SAC/NC	TMB	24.05	0.108	this work

[a]TAC: triple-atom catalyst. [b]DAC: dual-atom catalyst. [c]SAC: single-atom catalyst.

Table 2. Comparison of Oxidase-like Activity of FeCoZn-TAC/SNC with Other Catalysts[a]

catalysts	substrate	K_m (mM)	V_{max} (μM min^{-1})	ref
FeCoZn-TAC/SNC	TMB	0.459	13.38	this work
Fe-N-C-400[b]	TMB	0.269	20.28	33
nanoceria(*is*PNC)[c]	TMB	3.8	42	34
nano-CeO_2	TMB	0.42	6	35
Mn/PSAE[d]	TMB	0.11	4.2	36
MSN-AuNPs[e]	TMB	0.225	7.08	37
N-PCNSs-5[f]	TMB	0.095	0.18	38
Fe_3O_4	TMB	0.295	0.43	39
A-MIP[g]	TMB	0.316	0.3	39

[a]K_m and V_{max} are the Michaelis constant and the maximal reaction velocity, respectively. [b]Fe-N-C-400: Fe−N−C under carbonization 400 °C were synthesized. [c]*is*PNC: poly (acrylic acid). [d]PSAE: PEGylated single-atom enzyme. [e]MSN: Mesoporous silica. [f]N-PCNSs: N-doped porous carbon nanospheres. [g]A-^{MIP}: ABTS imprinted gels.

HAADF-STEM analysis reveals that the atomically dispersed iron, cobalt, and zinc species were atomically dispersed on the Fe, Co, and Zn sites located on the defect-rich and porous graphite structure (Figure 1c). In particular, the bright dots are recognized as well-isolated trimetallic sites, although there are still some individual Fe, Co, or Zn atoms (Figure 1d). Figure 1e shows the distribution of triple-metal atom sites at different angles corresponding to Figure 1d. The Fe, Co, and Zn content in the catalyst was 0.50, 0.48, and 0.53 at %, respectively, according to the coupled plasma optical emission spectrometry (ICP-OES) analysis (Table S1).

In addition, the Fourier transform EXAFS (FT-EXAFS) spectrum at the Fe K-edge (Figure 2a) shows a main peak at 1.5 Å for FeCoZn-TAC/SNC, which is consistent with the Fe−N peak of FePc and related to the backscattering between Fe and N atoms. In addition, there is a shoulder peak at 1.84 Å, which is attributed to the Fe−S bonds. For the Co K-edge FT-EXAFS spectrum of FeCoZn-TAC/SNC, a significant peak of about 1.47 Å is observed in Figure 2b, which corresponds to the Co−N scattering path. Figure 2c shows that the FT-EXAFS spectrum of FeCoZn-TAC/SNC at the Zn K-edge has a main peak at 1.47 Å, ascribed to Zn−N coordination. A quantitative EXAFS fitting to FeCoZn-TAC/SNC was performed to extract the Fe, Co, and Zn K-edge structural parameters. The fitting results are shown in Figure 2d−f, indicating that the fitted curves were in good agreement with the experimental spectra. According to the EXAFS analysis, the first shell of the central atom (Fe, Co, or Zn) shows a coordination number of three, four, and four, respectively, where Fe bonds with two N and one S atoms, and Co and Zn are connected to the other four N atoms, respectively, one of which is shared by both. Furthermore, a suitable model of the local configuration was constructed as in Figure 2g.

Oxidase-like Activity of FeCoZn-TAC/SNC and Its Reference Samples. We systematically studied the oxidase-like activity of FeCoZn-TAC/SNC and its reference samples. The oxidase/peroxidase-like catalytic activity of FeCoZn-TAC/SNC was verified through a typical chromogenic reaction with O_2/H_2O_2, where TMB was used as the substrate (Figure 3). The absorbance spectra show that the substrate was oxidized by the FeCoZn-TAC/SNC in the presence of O_2/H_2O_2. As a comparison, TMB was also employed to trigger chromogenic reactions (TMB + O_2 and TMB + H_2O_2) in the absence of FeCoZn-TAC/SNC, and the absorbance values were trivial. Michaelis−Menten kinetics was analyzed to explore the catalytic performance of FeCoZn-TAC/SNC and the reference samples toward TMB (Figures S1−S8 and 4a). The double-reciprocal Lineweaver−Burk plot for the oxidase-like activity of FeCoZn-TAC/SNC and these references (Figure 4b) also depicted the characteristic linear fit. The initial reaction rate of TMB oxidation was calculated from the kinetic curves, and FeCoZn-TAC/SNC exhibited the highest oxidase-like activity at 13.38 μM min^{-1} (Figure 4c). In addition, the experimental order of oxidase-like activity was FeCoZn-TAC/SNC > FeCoZn-TAC/NC > FeCo-DAC/NC > FeZn-DAC/NC > Fe-SAC/NC > CoZn-DAC/NC > Co-SAC/NC > Zn-SAC/NC (Table 1), indicating that the central three metal atoms and N and S coordination structures are crucial for the oxidase-like activity of

Table 3. Performance Comparison of the Developed Colorimetric Assay for AA Detection-Based on FeCoZn-TAC/SNC with Oxidase-like Activities and Other Reported AA Detection Methods

materials	linear range (μM)	LOD (μM)	method	ref
FeCoZn-TAC/SNC	0.01−90	0.006	colorimetric	this work
FeN_5 SA[a]/CNF	0−50	0.07	colorimetric	40
CNT/FeNC[b]	0.1−10	0.03	colorimetric	41
CoMo hybrids	0.5−50	0.25	colorimetric	42
SNC nanozymes	100−5000	80	colorimetric	8
GO[c]	0.5−1000	0.01	electrochemical	7
CuO/Pt nanocomposites	1−600	0.796	colorimetric	43
MOF[d]-808	30−1000	15	colorimetric	44

[a]FeN_5 SA: N-coordinated single-atom Fe. [b]CNT/FeNC: the single-atom nanozymes of carbon nanoframe-confined axial N-coordinated single-atom Fe. [c]GO: graphene oxide. [d]MOF: metal−organic framework.

https://doi.org/10.1021/acs.analchem.2c02853
Anal. Chem. 2022, 94, 14308−14316

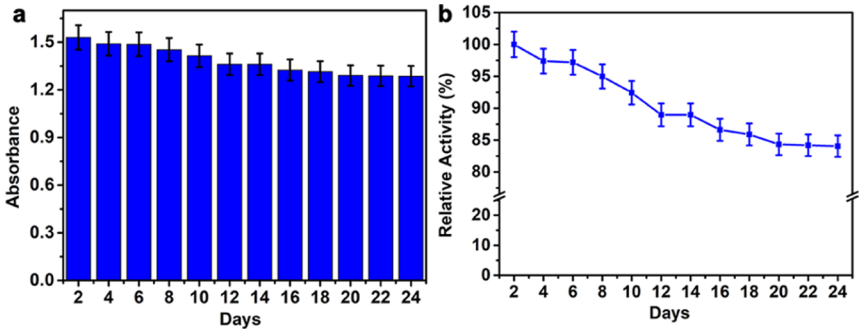

Figure 5. (a) Absorbance changes of FeCoZn-TAC/SNC-TMB-O_2 in the 24 day measurement; (b) time dependence of the relative activity of FeCoZn-TAC/SNC in the 24 day measurement.

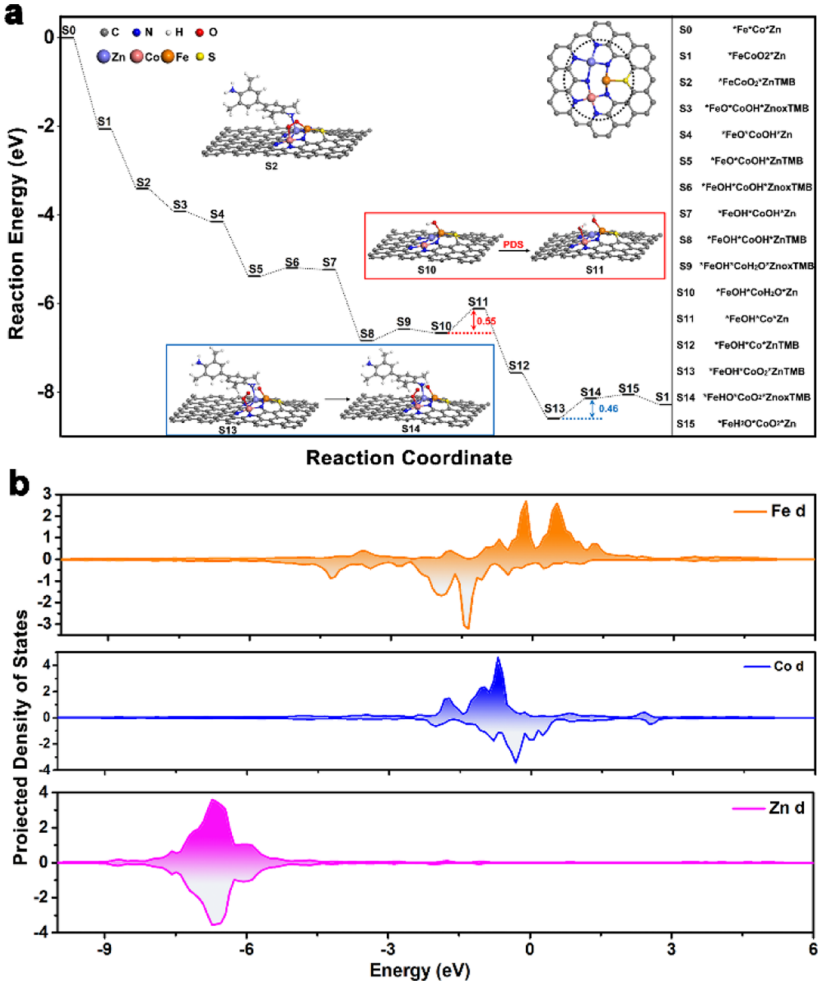

Figure 6. Theoretical oxidase-like performance of FeCoZn-TAC/SNC. (a) The energy evolution (eV) along the reaction coordinate is plotted with the structures of the FeCoZn-TAC/SNC (top right) and selected intermediates. The energy of the PDS is noted in red, with the corresponding structures drawn on the right. The most energy-consuming reaction on the Fe center is noted in blue, with the related structures illustrated at the bottom left. (b) Predicted PDOS of d bands for the three metal centers (Fe, Co, and Zn) in the FeCoZn-TAC/SNC system.

FeCoZn-TAC/SNC. The synergistic effect of these factors resulted in the superior oxidase-like properties of FeCoZn-TAC/SNC. The detailed kinetics parameters [Michaelis–Menten constant (K_m) and the maximal reaction velocity (V_{max})] were acquired from the kinetics plot and are listed in Table 1. Thereinto, especially the lower K_m and the higher V_{max} values of FeCoZn-TAC/SNC indicated a higher affinity of FeCoZn-TAC/SNC active centers toward TMB and more impressive catalytic efficiency compared to various reported nanozymes (Table 2). The sensing principle is illustrated in Figure 4d. In the presence of oxygen, FeCoZn-TAC/SNC catalyzes the oxidation of TMB to form a blue substance (oxTMB). The presence of AA inhibits the formation of oxTMB, making the blue solution lighter. FeCoZn-TAC/SNC with the oxidase-like activity (Figure 3) catalyzes the rapid oxidation of TMB by O_2 to generate the oxidation product (oxTMB) and reactive oxygen species ($^{\bullet}O_2^-$) (Figure 4e). The oxTMB then reacts with AA to regenerate TMB. The addition of

https://doi.org/10.1021/acs.analchem.2c02853
Anal. Chem. 2022, 94, 14308−14316

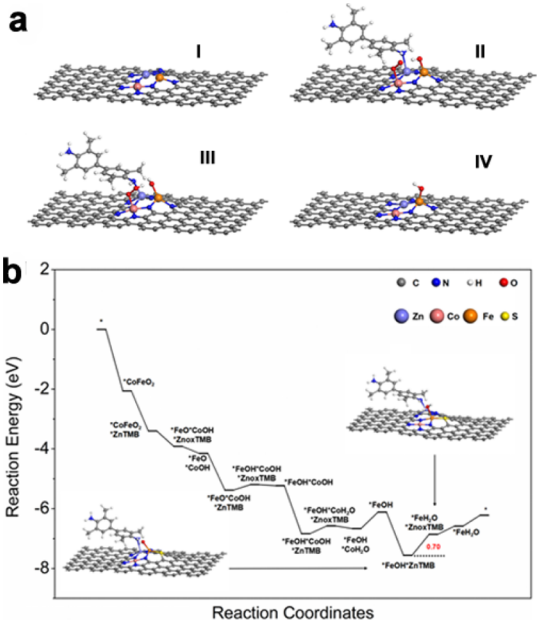

Figure 7. (a) Optimized structures for FeCoZn-TAC/SNC related intermediates (I) clean surface; (II) *(Zn)TMB*Fe(OH)*Co(O_2); (III) *(Zn)oxTMB*Fe(OH)*Co(OOH); and (IV) *(Fe)OH. (b) Reaction energy plot along the A12−A15 pathway. The energy for the PDS is denoted in red with the corresponding structures illustrated.

AA with different concentrations to FeCoZn-TAC/SNC-TMB-O_2 reaction mixtures clearly results in variations in the oxTMB product, in the UV−vis spectrum with a decreased absorption at 652 nm (Figure 4f), and in terms of the solution color (from dark blue to light blue) (inset of Figure 4g).

Ascorbic Acid Sensing. Under optimal conditions (Figures S9−S11), a linear calibration curve was obtained from the absorbance change at 652 nm as a function of AA concentration spanning a range of 0.01−90 μM, with 0.99 of R^2 (Figure 4g). The detection limit of AA reached as low as 6.24 nM according to 3σ rule. The high sensitivity of this colorimetric assay was attributed to the superior oxidase properties of FeCoZn-TAC/SNC. Most importantly, FeCoZn-TAC/SNC-based colorimetric assay exhibits a higher sensitivity when compared with other optical/electrochemical AA sensors in Table 3. Likewise, the selectivity of the FeCoZn-TAC/SNC-TMB-O_2 hybrid system was explored with common metal ions and biological molecules, each at a concentration of 1 mM (Figures S12 and 4h). Unsurprisingly, only 100 μM AA led to a notable absorbance change, and no distinct absorbance changes were observed for interfering substances, manifesting a good selectivity of the colorimetric assay. Encouraged by the excellent sensitivity and selectivity of this assay, the performance of this assay in 100-fold diluted human serum samples was tested (Figures S13 and 4i). The serum used in this work was from the patient serum of PLA General Hospital. The colorimetric response obtained from AA was nearly identical in serum versus in deionized water, verifying that this sensing strategy had excellent performance in real sample analysis. In addition, the catalytic stability result of FeCoZn-TAC/SNC showed that the catalytic activity was reduced only by 20% of the original value after 24 days (Figure 5), implying the relatively high stability.

DFT Calculations. The reaction mechanisms were examined theoretically with DFT (Figures 6, 7, and S14, Tables S2 and S3). The thermodynamically favored energy evolution along the reaction coordinate is plotted in Figure 6a with the proposed reactions (A1−A15, B1−B4) listed in Table S2. To determine the best possible adsorption sites of O_2 molecule, the projected density of state (PDOS) analysis of the metal centers was carried out, with the results shown in Figure 6b. It is clear that the d bands for Co and Fe centers are close to the Fermi level, indicating their strong binding with O_2. As to the Zn center, though weaker for O-binding, it serves as a possible adsorption site for the N atom of the TMB molecule. The reaction starts with O_2 adsorption, and a Co−O−O−Fe bridge structure (S1) is formed. Meanwhile, TMB adsorbs on the Zn site. Thus, our FeCoZn-TAC design brings both O_2 and TMB near to the catalyst as shown on the top left of Figure 6a (S2), facilitating the reactions. Furthermore, strong interactions between the active metal center and O_2/TMB stretch both O−O and N−H bonds, activating the two molecules. It promotes the H transferred from $-NH_2$ to the O atom, forming oxTMB. The following desorption of oxTMB benefits greatly from the protonation of the −NH group (A4). More TMB molecules are oxidized similarly until the complete reduction of the adsorbed O_2 to H_2O. The oxygen atom on the Co site is predicted to be reduced and desorbed as H_2O. However, the strong Fe−O interaction results in high energy demand for further reduction of Fe−OH to Fe−OH_2 (Figure 7b). Correspondingly, another O_2 molecule can easily adsorb onto the Co site as *FeOH*CoO_2*ZnTMB (S13). The hydrogen bond between the H atom of *FeOH and the O atom of *CoO_2 then facilitates the H-transfer from $-NH_2$ to Fe−OH and decreases the reaction energy from 0.70 to 0.46 eV (reaction B2 in Table S2). After the desorption of H_2O from the Fe site, the adsorbed O_2 simultaneously relaxes to the Co−O−O−Fe bridge geometry (S1). The potential-determining step (PDS) along this pathway is the H_2O desorption from the Co center (reaction A11, 0.55 eV), demonstrating good catalytic activity of our TAC. The effects of S/N doping aside from Fe were investigated by comparing the most energy-consuming step on Fe as noted in Figure 6a (in blue, reaction B2). The reaction energy with N is 0.64 eV, higher than 0.46 eV with S. The lower electronegativity of S alleviates the electron depletion of Fe, weakening the Fe−OH binding (Fe−O distance is 1.815 Å with S, 1.780 Å with N), making the O atom more easily react with the TMB. Consequently, the substitution of Fe−N with Fe−S further improves the catalytic performance of TAC.

■ CONCLUSIONS

In summary, we report the first example of ZnCoFe TAzymes with splendid oxidase-like activity, because they can promote the rapid oxidation of TMB in slightly acidic conditions without the aid of H_2O_2. Serving as an effective nanocatalyst, ZnCoFe TAzyme exhibits high catalytic activities toward the chromogenic reaction between TMB and O_2. The underlying mechanism of the ZnCoFe TAzyme as an oxidase-like catalyst is closely related to the Zn−Co−Fe synergy effect. A proof-of-concept colorimetric detection system for AA sensing was developed, which exhibited an LOD of 6.24 nM and extraordinary anti-interference ability. Impressively, the AA detection result in deionized water was consistent with that of this method in spiked human serum. Taken together, the current work not only offers a facile approach to synthesize TAzymes with the oxidase-like activity but also opens an innovative method to constructing facile biosensors..

https://doi.org/10.1021/acs.analchem.2c02853
Anal. Chem. 2022, 94, 14308−14316

■ ASSOCIATED CONTENT

Supporting Information

The Supporting Information is available free of charge at https://pubs.acs.org/doi/10.1021/acs.analchem.2c02853.

Time-dependent absorbance changes corresponding to the FeCoZn-TAC/SNC, FeCoZn-TAC/NC, FeZn-DAC/NC, CoZn-DAC/NC, FeCo-DAC/NC, Fe-SAC/NC, Co-SAC/NC, and Zn-SAC/NC-catalyzed oxidation of TMB by O_2 using different concentrations of TMB, optimal conditions, UV−vis absorption spectra of the FeCoZn-TAC/SNC-TMB-O_2 reaction system toward AA at 0.1 mM and interferents, UV−vis absorption spectra of the FeCoZn-TAC/SNC-TMB-O_2 reaction system toward different concentrations of AA in serum, cluster cut from the periodic FeCoZn-TAC/SNC model, calculated bond lengths around the metal centers in the FeCoZn-TAC/SNC system, and reaction mechanism on FeCoZn-TAC/SNC catalyst for TMB oxidation, along with the reaction type tagged after each step (PDF)

■ AUTHOR INFORMATION

Corresponding Authors

Ting Tan − *Laboratory of Theoretical and Computational Nanoscience, CAS Center for Excellence in Nanoscience, National Center for Nanoscience and Technology, Chinese Academy of Sciences, Beijing 100190, China;* orcid.org/0000-0003-3129-8113; Phone: +86-010-68903047; Email: tant@nanoctr.cn

Wenxing Chen − *Energy & Catalysis Center, School of Materials Science and Engineering, Beijing Institute of Technology, Beijing 100081, China;* orcid.org/0000-0001-9669-4358; Email: wxchen@bit.edu.cn

Zhengbo Chen − *Department of Chemistry, Capital Normal University, Beijing 100048, China;* orcid.org/0000-0002-9443-7929; Email: czb979216@sina.com

Authors

Rufen Wu − *Department of Chemistry, Capital Normal University, Beijing 100048, China*

Mengru Sun − *Energy & Catalysis Center, School of Materials Science and Engineering, Beijing Institute of Technology, Beijing 100081, China*

Xiaolong Liu − *Laboratory of Theoretical and Computational Nanoscience, CAS Center for Excellence in Nanoscience, National Center for Nanoscience and Technology, Chinese Academy of Sciences, Beijing 100190, China*

Fengjuan Qin − *Energy & Catalysis Center, School of Materials Science and Engineering, Beijing Institute of Technology, Beijing 100081, China*

Xinyu Zhang − *Department of Chemistry, Capital Normal University, Beijing 100048, China*

Zhenni Qian − *Department of Chemistry, Capital Normal University, Beijing 100048, China*

Juan Huang − *Department of Chemistry, Capital Normal University, Beijing 100048, China*

Yujing Li − *Energy & Catalysis Center, School of Materials Science and Engineering, Beijing Institute of Technology, Beijing 100081, China;* orcid.org/0000-0001-5440-5343

Complete contact information is available at: https://pubs.acs.org/10.1021/acs.analchem.2c02853

Author Contributions

#R.W., M.S., and X.L. contributed equally to this work.

Notes

The authors declare no competing financial interest.

■ ACKNOWLEDGMENTS

All authors gratefully acknowledge the financial support from the Scientific Research Project of Beijing Educational Committee (KM202010028007) and the Natural Science Foundation of China (52171157).

■ REFERENCES

(1) Kim, D. O.; Lee, C. Y. *Crit. Rev. Food Sci. Nutr.* **2004**, *44*, 253−273.
(2) Weeks, B. S.; Perez, P. P. *Med. Sci. Mon.* **2007**, *13*, 205−210.
(3) Peterkofsky, B.; Udenfriend, S. *Proc. Natl. Acad. Sci. U.S.A.* **1965**, *53*, 335−342.
(4) Abudu, N.; Miller, J. J.; Attaelmannan, M.; Levinson, S. S. *Clin. Chim. Acta* **2004**, *339*, 11−25.
(5) Li, L.; Wang, C.; Liu, K.; Wang, Y.; Liu, K.; Lin, Y. *Anal. Chem.* **2015**, *87*, 3404−3411.
(6) Feng, L. L.; Wu, Y. X.; Zhang, D. L.; Hu, X. X.; Zhang, J.; Wang, P.; Song, Z. L.; Zhang, X. B.; Tan, W. H. *Anal. Chem.* **2017**, *89*, 4077−4084.
(7) Jiang, Y.; Xiao, X.; Li, C.; Luo, Y.; Chen, S.; Shi, G.; Han, K.; Gu, H. *Anal. Chem.* **2020**, *92*, 3981−3989.
(8) Chen, Y.; Jiao, L.; Yan, H.; Xu, W.; Wu, Y.; Wang, H.; Gu, W.; Zhu, C. *Anal. Chem.* **2020**, *92*, 13518−13524.
(9) Matsuoka, Y.; Yamato, M.; Yamasaki, T.; Mito, F.; Yamada, K. I. *Free Radical Biol. Med.* **2012**, *53*, 2112−2118.
(10) Song, W.; Duan, W.; Liu, Y.; Ye, Z.; Chen, Y.; Chen, H.; Qi, S.; Wu, J.; Liu, D.; Xiao, L.; Ren, C.; Chen, X. *Anal. Chem.* **2017**, *89*, 13626−13633.
(11) Wang, Q.; Zhang, S.; Zhong, Y.; Yang, X.-F.; Li, Z.; Li, H. *Anal. Chem.* **2017**, *89*, 1734−1741.
(12) Ding, H.; Yu, S.; Wei, J.; Xiong, H. M. *ACS Nano* **2016**, *10*, 484−491.
(13) Masud, M. K.; Yadav, S.; Islam, M. N.; Nguyen, N. T.; Salomon, C.; Kline, R.; Alamri, H. R.; Alothman, Z. A.; Yamauchi, Y.; Hossain, M. S. A.; Shiddiky, M. J. A. *Anal. Chem.* **2017**, *89*, 11005−11013.
(14) Bhattacharjee, R.; Tanaka, S.; Moriam, S.; Masud, M. K.; Lin, J. J.; Alshehri, S. M.; Ahamad, T.; Salunkhe, R. R.; Nguyen, N. T.; Yamauchi, Y.; Hossain, M. S. A.; Shiddiky, M. J. A. *J. Mater. Chem. B* **2018**, *6*, 4783−4791.
(15) Masud, M. K.; Kim, J.; Billah, M. M.; Wood, K.; Shiddiky, M. J. A.; Nguyen, N. T.; Parsapur, R. K.; Kaneti, Y. V.; Alshehri, A. A.; Alghamidi, Y. G.; Alzahrani, K. A.; Adharvanachari, M.; Selvam, P.; Hossain, M. S. A.; Yamauchi, Y. *J. Mater. Chem. B* **2019**, *7*, 5412−5422.
(16) Masud, M. K.; Na, J.; Younus, M.; Hossain, M. S. A.; Bando, Y.; Shiddiky, M. J. A.; Yamauchi, Y. *Chem. Soc. Rev* **2019**, *48*, 5717−5751.
(17) Jiang, D. W.; Ni, D. L.; Rosenkrans, Z. T.; Huang, P.; Yan, X. Y.; Cai, W. B. *Chem. Soc. Rev.* **2019**, *48*, 3683−3704.
(18) Qiao, B.; Wang, A.; Yang, X.; Allard, L. F.; Jiang, Z.; Cui, Y.; Liu, J.; Li, J.; Zhang, T. *Nat. Chem.* **2011**, *3*, 634−641.
(19) Zhang, J.; Wu, X.; Cheong, W. C.; Chen, W. X.; Lin, R.; Li, J.; Zheng, L. R.; Yan, W. S.; Gu, L.; Chen, C.; Peng, Q.; Wang, D. S.; Li, Y. *Nat. Commun.* **2018**, *9*, 1002.
(20) Gao, C.; Chen, S. M.; Wang, Y.; Wang, J. W.; Zheng, X. S.; Zhu, J. F.; Song, L.; Zhang, W. K.; Xiong, Y. J. *Adv. Mater.* **2018**, *30*, 1704624.
(21) Ji, S.; Chen, Y.; Wang, X.; Zhang, Z.; Wang, D.; Li, Y. *Chem. Rev.* **2020**, *120*, 11900−11955.
(22) Hannagan, R. T.; Giannakakis, G.; Flytzani-Stephanopoulos, M.; Sykes, E. C. H. *Chem. Rev.* **2020**, *120*, 12044−12088.
(23) Liu, L.; Corma, A. *Chem. Rev.* **2018**, *118*, 4981−5079.
(24) Jiao, L.; Yan, H.; Wu, Y.; Gu, W.; Zhu, C.; Du, D.; Lin, Y. *Angew. Chem., Int. Ed.* **2020**, *59*, 2565−2576.
(25) Wang, A.; Li, J.; Zhang, T. *Nat. Rev. Chem* **2018**, *2*, 65−81.
(26) Kresse, G.; Furthmüller, J. *Comp. Mater. Sci.* **1996**, *6*, 15−50.

(27) Kresse, G.; Hafner, J. *Phys. Rev. B: Condens. Matter Mater. Phys.* **1994**, *49*, 14251−14269.
(28) Kresse, G.; Hafner, J. *Phys. Rev. B: Condens. Matter Mater. Phys.* **1993**, *47*, 558.
(29) Kresse, G.; Furthmüller, J. *Phys. Rev. B: Condens. Matter Mater. Phys.* **1996**, *54*, 11169−11186.
(30) Perdew, J. P.; Burke, K.; Ernzerhof, M. *Phys. Rev. Lett.* **1996**, *77*, 3865−3868.
(31) Grimme, S.; Antony, J.; Ehrlich, S.; Krieg, H. *J. Chem. Phys.* **2010**, *132*, 154104.
(32) Grimme, S.; Ehrlich, S.; Goerigk, L. *J. Comput. Chem.* **2011**, *32*, 1456−1465.
(33) Xu, Y.; Xue, J.; Zhou, Q.; Zheng, Y.; Chen, X.; Liu, S.; Shen, Y.; Zhang, Y. *Angew. Chem., Int. Ed.* **2020**, *59*, 14498−14503.
(34) Asati, A.; Santra, S.; Kaittanis, C.; Nath, S.; Perez, J. M. *Angew. Chem., Int. Ed.* **2009**, *121*, 2344−2348.
(35) Cheng, H.; Lin, S.; Muhammad, F.; Lin, Y. W.; Wei, H. *ACS Sens.* **2016**, *1*, 1336−1343.
(36) Zhu, Y.; Wang, W.; Cheng, J.; Qu, Y.; Dai, Y.; Liu, M.; Yu, Y.; Wang, C.; Wang, H.; Wang, S.; Zhao, C.; Wu, Y.; Liu, Y. *Angew. Chem., Int. Ed.* **2021**, *133*, 9566−9574.
(37) Tao, Y.; Ju, E.; Ren, J.; Qu, X. *Adv. Mater.* **2015**, *27*, 1097−1104.
(38) Fan, K.; Xi, J.; Fan, L.; Wang, P.; Zhu, C.; Tang, Y.; Gao, L. *Nat. Commun.* **2018**, *9*, 1440.
(39) Zhang, Z.; Zhang, X.; Liu, B.; Liu, J. *J. Am. Chem. Soc.* **2017**, *139*, 5412−5419.
(40) Huang, L.; Chen, J.; Gan, L.; Wang, J.; Dong, S. *Sci. Adv.* **2019**, *5*, 5490.
(41) Cheng, N.; Li, J. C.; Liu, D.; Lin, Y.; Du, D. *Small* **2019**, *15*, 1901485.
(42) Ding, Y.; Wang, G.; Sun, F.; Lin, Y. *ACS Appl. Mater.* **2018**, *10*, 32567−32578.
(43) Wang, X.; Han, Q.; Cai, S.; Wang, T.; Qi, C.; Yang, R.; Wang, C. *Analyst* **2017**, *142*, 2500−2506.
(44) Zheng, H. Q.; Liu, C. Y.; Zeng, X. Y.; Chen, J.; Lü, J.; Lin, R. G.; Cao, J. W.; Lin, Z.-J.; Su, J.-W. *Inorg. Chem.* **2018**, *57*, 9096−9104.

https://doi.org/10.1021/acs.analchem.2c02853
Anal. Chem. 2022, 94, 14308−14316